Journal Name

ARTICLE TYPE

Cite this: DOI: 10.1039/xxxxxxxxxx

Shear-Banding due to Polymer Entanglements: Sharp and Broad Shear-Band Interfaces in Xanthan Solutions†

Hu Tang,[ab] Tatiana Kochetkova,[ac] Hartmut Kriegsand,[a] Jan K. G. Dhont[ad] and Pavlik Lettinga*[ab]

Received Date
Accepted Date

DOI: 10.1039/xxxxxxxxxx

www.rsc.org/journalname

We report on the smooth transition between the classic shear-banding instability and curved flow profiles, both resulting from strong shear-thinning dispersions of concentrated xanthan (a highly charged poly-saccharide). Pronounced shear-banded flow, where two extended shear-bands are separated by a relatively sharp interface, is observed in a limited range of shear rates, at very low ionic strength and at a high concentration, using heterodyne light scattering to measure spatially resolved velocity profiles. The width of the interface between the coexisting shear-bands broadens to span a sizable fraction of the gap of the shear cell, either by changing the shear rate, by lowering the concentration, or by increasing the ionic strength. The broadening results in a smooth transition to highly curved flow profiles and is connected to a disappearing flow birefringence. Thus, these experiments show that the classic shear-banding instability can give rise to highly curved flow profiles, due to the existence of broad interfaces between the bands, with an extent of the order or larger than the cell gap width. This observation may resolve the ongoing dispute concerning shear-banding of highly entangled polymeric systems, suggesting that the curved flow profiles that have been observed in the past are in fact shear-banded states with an unusually broad interface.

1 Introduction

Complex fluids often display flow instabilities at low Reynolds numbers due to flow induced changes in micro-structural order. Especially gradient shear-banding is ubiquitous in complex fluids, where two regions (the "bands") coexist within a well-defined range of applied shear rates, and where the shear rates within the bands are essentially independent of position[1–3]. Shear-banding is often related to extreme shear thinning, where the shear viscosity strongly decreases with increasing shear rate.* From the standard form of the Navier-Stokes equation it can be shown that a homogeneous, non-banded flow profile is unstable when the stress σ_{hom} of the uniformly sheared system (before shear-banding sets in) decreases with increasing shear rate $\dot{\gamma}$, that is, when $d\sigma_{hom}/d\dot{\gamma} < 0$ (see, for example, Refs.[5–8]). In the range of applied shear rates where such strong shear thinning occurs, the *stationary state* is a gradient banded flow, for which the stress is independent of the applied shear rate. The flow curve (the stress plotted against the applied shear rate) thus exhibits a stress plateau. The stress plateau can be sloped, however, due to polydispersity, shear-induced mass transport, and/or a variation in, for example, orientational order[4,9,10].

The hallmark of shear-banding systems are wormlike micelles, which can be considered as stiff and living polymers. In these systems shear can induce breakage of the constitutive chains as well as alignment[11–16], which both contribute to the stress relaxation required for strong shear thinning. Breakage and alignment also play important roles in shear-banding hydrogen-bonded supramolecular polymers[17], while shear-banding in dispersions of actin filaments[18] and block-copolymer wormlike micelles[19,20] is caused by alignment and shear-banding in associative polymer networks[21] is caused by breakage. Whether shear-banding is a generic phenomenon for the more common case of entangled polymeric systems is still under debate. Indeed, stress plateaus for polymeric systems are generally not very pronounced[22,23], while the shape of the measured flow curves is very sensitive of the experimental conditions[24–26]. Shear-banded states for entangled polymers have been reported, but again

[a]ICS-3, Forschungszentrum Jülich GmbH, 52428 Jülich, Germany. E-mail: p.lettinga@fz-juelich.de
[b]Laboratory for Soft Matter and Biophysics, KU Leuven, B-3001 Leuven, Belgium.
[c]Department of biophysics, Belarussian State University, 220000 Minsk, Belarussia.
[d]Heinrich-Heine Universität Düsseldorf, Fakultät Physik, Düsseldorf, Germany.
†Electronic Supplementary Information (ESI) available. See DOI:10.1039/b0000x/
* For systems with a yield stress, shear-banding can also occur due to shear-gradient induced mass transport, without any shear thinning[4].

this very much depends on the experimental conditions. Shear-banding is mainly observed as a transient state in LAOS (Large Amplitude Oscillation Shear) and startup experiments on polybutadiene[27–30] and DNA solutions[31–34]. For these systems shear-banding does occur under steady shear conditions after start up, but for DNA it could be suppressed by a ramp-up or quench down shear protocol. Therefore, it has been suggested that these stationary shear-banded states are meta-stable[34]. Control experiments on entangled polybutadiene and polystyrene reported in Refs.[35–38] even showed that there is no shear-banding neither in transient nor steady state. Moreover, no clear shear-banded flow profiles are observed in many of the experiments where shear-banding is claimed, but rather highly curved profiles. Such curved flow profiles can also occur, however, when shear-banding is absent, for example due to the stress gradient in a Couette cell in combination with a strong shear thinning fluid.

The aim of the present paper is to clarify if highly entangled polymeric systems can exhibit the classic shear-banding instability that complies with strong shear thinning, without necessarily giving rise to a clear shear-banded state but rather to a highly curved flow profile. For our study we use xanthan, a highly charged poly-saccharide, as a shear-thinning polymer. The beauty of this system is that its rheology is highly tunable[39–44], especially by changing the ionic strength. For this reason, xanthan is used in abundance as a food additive and rheology modifier in food industry[45], so that it is also of practical importance to understand the flow behaviour of xanthan solutions. The effect of ionic strength on shear-band formation has already been identified for entangled DNA solutions, suggesting that electro-static repulsion facilitates shear-induced alignment and in this way enhances shear-banding[46]. Such local interactions and molecular features can possibly be related to shear banding via the convective-constraint-release theory[47] as first introduced in Ref.[48]. The theory accounts for both diffusion of polymer chains through a confining tube as well as flow-induced convection of the tube, leading to a non-monotonous constitutive equation[7,49]. Alternatively, the shear-banding mechanism for entangled polymers has been interpreted as force imbalance between intermolecular griping force and elastic retraction force[50]. We conjecture that the local interactions change dramatically for xanthan as the electrostatic repulsion as well as the stiffness of xanthan changes with ionic strength (the persistence length varies from 417 nm in pure water to 150 nm in $0.1-0.5\ M\ KCl$[51]) .

Indeed, we will unambiguously identify shear-banding at very low ionic strength, at a high concentration and in a range of relatively low applied shear rates, as in this region the observed stationary flow profiles consist of two spatially extended regions (the "bands"), within which the shear rate is essentially independent of position, and which are separated by a relatively sharp interface. An unexpected increase of the width of the interface, for which we will give a new definition, is observed when moving away from this region in parameter space. We find highly curved flow profiles when the extent of the interface is comparable or larger than the cell gap width, despite the fact that the system exhibits the classic shear-banding instability (for which $d\sigma_{hom}/d\dot{\gamma} < 0$). To avoid confusion, we shall refer to a stationary velocity profile as a SBI-state (where "SBI" stands for "Shear-Banding Instability"), when the system, for the applied shear rate, exhibits the classic shear-banding instability. A SBI-state can thus be a shear-banded state, in the sense that there are two clear bands within which the shear rate is constant, separated by a sharp interface, or it can be a highly curved profile for broad interfaces comparable or larger than the gap width. The question raised above is thus whether the observed highly curved flow profiles correspond to SBI-states.

This paper is organized as follows. Section 2 contains details on the materials and methods used in this study. Section 3 presents the rheology of samples with different xanthan and salt concentrations. The flow profiles for these samples and the identification of shear-banding are discussed in section 4. In section 5 a diagram-of-states is constructed, and results on birefringence measurements are presented. A discussion and conclusions are given in section 6.

2 Materials and Methods

Xanthan powder was purchased from Sigma and used without further purification. To prepare aqueous xanthan solutions with concentrations of 0.3, 0.5, and 0.7 $wt\%$, the powder was predissolved in mini Q water and mixed for 30 min at room temperature. The resultant solution was then heated to 95 ^oC, kept at that temperature for one hour, and subsequently gradually cooled down to room temperature. For the 0.7 $wt\%$ sample we added NaCl to a final ionic strength of 5 mM, 10 mM and 1 M, which tunes the flexibility of the polymer backbone as well as the electro-static repulsion between the polymers. The system is not a perfect model system, in the sense that it can be branched to an unknown extent due to pair mismatch, and it is polydisperse, so that we do not have access to the number of entanglements (the degree of branching might aid shear-band formation, as was shown for star polymers[52,53]).

Rheological measurements were carried out using an ARES rheometer (Rheometric Scientific Inc., NJ) operating at 20 ^oC with a cone-plate geometry, with a cone angle of 0.04 rad, diameter of 25 mm and a gap distance of 0.046 mm. To prevent water evaporation during rheological measurements, the meniscus of the aqueous xanthan solution in the cone-plate cell was surrounded by anti-evaporation silicone oil (Ibidi).

Flow velocity profiles were obtained at 20 ^oC with a heterodyne light scattering set up specially designed for this purpose. Here, two focused laser beams are crossed at a point within the gap of an optical Couette cell. The local velocity at the point where the two lasers cross is determined from the time-period of oscillation of the internsity-correlation function of the scattered light from both beams in the forward direction. The position of the point where the laser beams cross is varied to scan the entire gap, thus enabling the measurement of flow profiles. The reported local velocities at each point are averages over at least three measurements. A detailed decription of the set up can be found in Ref.[54]. The optical Couette cell is coupled to a motor for controlling the rotational speed of the inner cylinder. The shear cell has a gap width of 1.5 mm, with cylinder diameters of 45 mm and 48 mm.

In order to gain structural information of the sample during shear, the intensity of a separate laser beam passing through the

sample, placed between two crossed polarizers, is measured by means of a diode. Moreover, images of the sample during steady shear were taken between two crossed sheet polarizers using a white light box in order to probe the birefringent structure.

3 Rheology

Figure 1 shows the storage G' and loss modulus G'' as well as the shear-rate dependence of the stress in the stationary state of xanthan solutions at different concentrations and ionic strengths. For the samples without salt, both the storage G' and loss modulus G'' increase with concentration, while the crossover frequency decreases dramatically, as can be seen in Fig.1a. The corresponding much slower chain dynamics at higher concentrations is attributed to an increasing degree of entanglement. The flow curve is similarly sensitive to the xanthan concentration, going from an almost Newtonian flow curve at $0.3\ wt\%$ xanthan to a strongly shear-thinning flow curve with a sloped stress plateau at $0.7\ wt\%$ xanthan, as seen in Fig.1b.

The rheological properties are much less sensitive to the ionic strength, as can be seen from Figs.1c,d, for the $0.7\,wt\%$ sample. There is a slight shift of the crossover frequency to smaller frequencies on increasing salt concentration. This is attributed to an increasing xanthan-chain flexibility as the Debye length decreases, leading to a slight increased degree of entanglement. The flow curves (the stress as a function of the applied shear rate) shown in Fig.1d are equally similar for each of the salt concentrations. There is a sloped plateau for all salt concentrations within the shear-rate range of about $1-100\,s^{-1}$, where the stress σ varies with the shear rate $\dot{\gamma}$ as $\sigma \sim \dot{\gamma}^{m_{fc}}$, with the exponent $m_{fc} \approx 0.20$ (the index "fc" stands for "flow curve"), indicative for strong shear-thinning.

As can be seen from Fig.2, we obtain a master curve for G' and G'' by just rescaling the frequency. This implies that the dynamics of the various xanthan solutions underly the same mechanisms, independent of the xanthan concentration and the salt concentration. There is no change in the principle processes that set the dynamics of these systems on changing either the xanthan or the salt concentration. The degree of entanglement changes with xanthan and salt concentration, but the entanglement-relaxation mechanisms remain the same. Possible differences in shear-banding behaviour can therefore not be attributed to fundamental structural changes.

4 Velocity Profiles

The sloped stress plateaus observed in the flow curves in Fig.1d for the $0.7\,wt\%$ samples hints to the possibility of shear-banding resulting from strong shear-thinning. This is confirmed for the sample with no added salt in Fig.3, where the local velocity is plotted as a function of the position within the gap of the optical Couette cell, for small shear rates ($5-50\,s^{-1}$) in Fig.3a, and for higher shear rates ($50-130\,s^{-1}$) in Fig.3b. There is no sign of slip for this sample, nor for any of the remaining samples that will be discussed later. Shear-banding does not occur below shear rates of about $15\,s^{-1}$ (see Fig.3a) and above shear rates of $115\,s^{-1}$ (see Fig.3b). This shear-rate range lies within the range where the sloped plateau in the flow curve in Fig.1d is found. This is

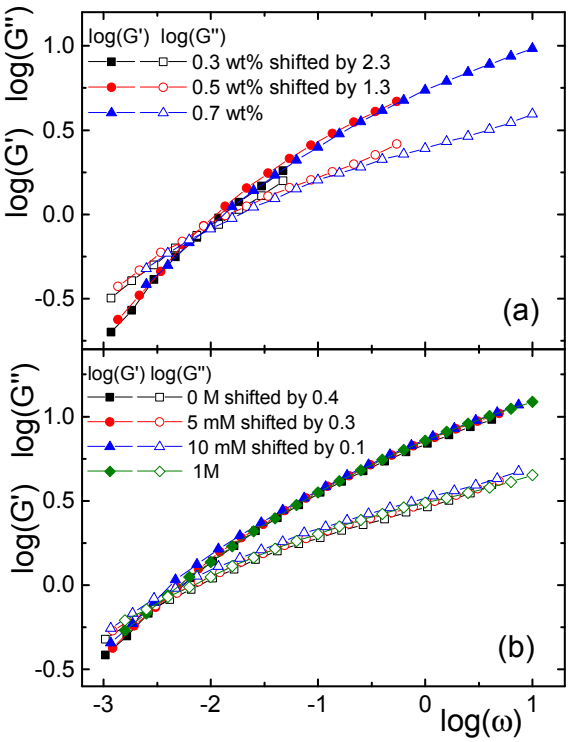

Fig. 2 Master curves for the storage G' and loss modulus G'' by (a) time-concentration and (b) time-ionic strength superposition. The shifts of the logarithmic frequency scale are indicated in the figures.

a strong indication that the banded flow profiles in Fig.3 are related to the classic shear-banding instability, being due to very strong shear-thinning. Shear-banding profiles with well-defined regions of constant shear rate, separated by a relatively sharp interface, are observed for shear rates between $15-50\,s^{-1}$ (see Fig.3a). At higher shear rates, however, the profiles gradually become more curved, without a sharp interface (see Fig.3b). The question then arises whether these curved flow profiles are still due to the shear-banding instability, but with a very broad interface, or whether other mechanisms play a role leading to such curved profiles. However, from the smooth transition of banded profiles with a sharp interface to curved profiles, it seems that the curved profiles are banded flows with a broad interface. The stationary states within the shear-rate range of about $15-115\,s^{-1}$ are thus most probably SBI-states, as defined at the end of the introduction. The more detailed analysis given below confirms this conjecture.

Velocity profiles for all investigated samples, with varying xanthan and added-salt concentrations, are given in Fig.4a-e. Except for the sample of $0.7\,wt\%$ without added salt (for which a magnification of Fig.4a is given in Fig.3), we observed no band-formation with sharp interfaces. Instead highly curved flow profiles are observed. Also here the question is whether or not these highly curved flow profiles correspond to SBI-states with a broad interface.

In order to decide whether the curved flow profiles correspond to SBI-states, we first consider the construction of the lever rule. The lever rule is based on the following consideration. In the

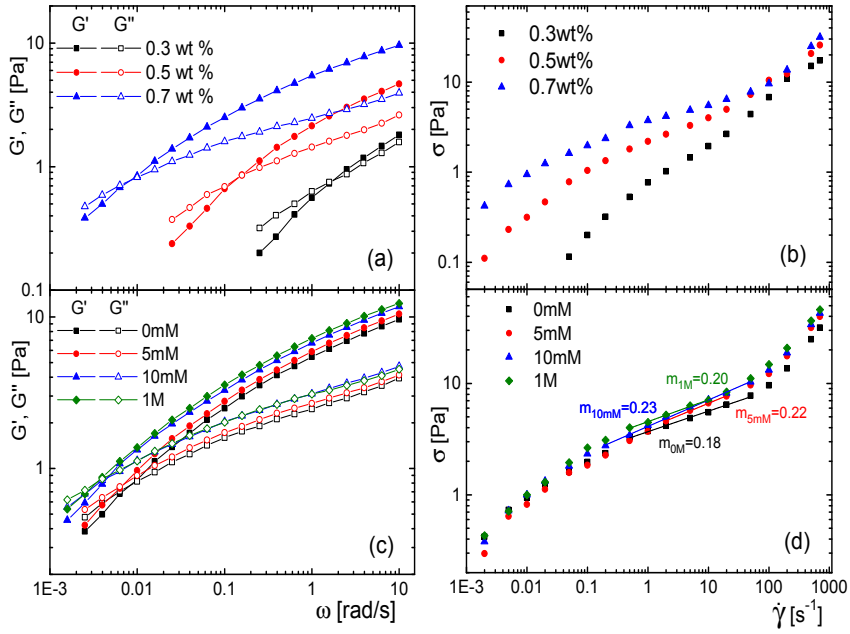

Fig. 1 (a) The storage G' and loss modulus G'' and (b) the stress σ in the stationary state as a function of the shear rate $\dot{\gamma}$, for various xanthan concentrations without added salt. (c) The same as in (a), and (d) the same as in (b), but now for various salt concentrations at a fixed xanthan concentration of $0.7 wt\%$. The lines in (d) indicate the sloped stress plateaus, with an indication of the shear-thinning exponent m_{fc} for the various xanthan concentrations, which is defined as $\sigma \sim \dot{\gamma}^{m_{fc}}$.

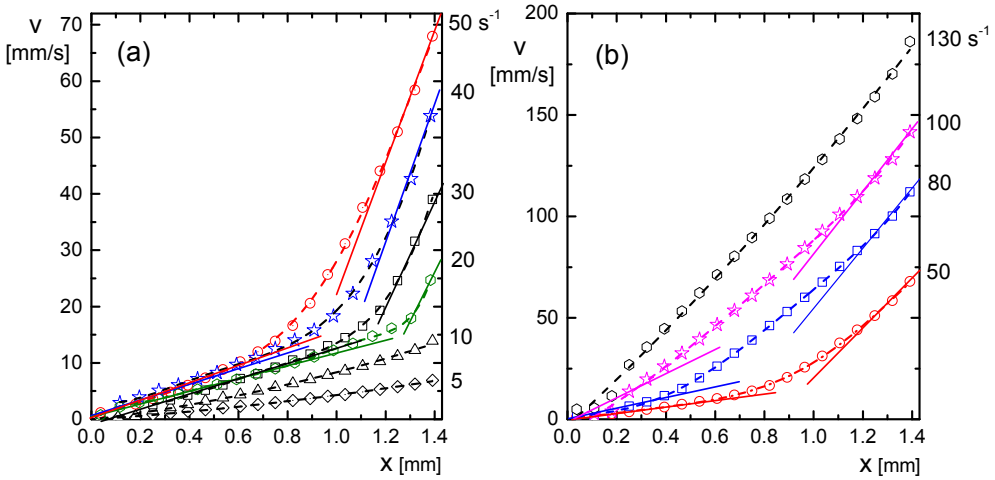

Fig. 3 The suspension velocity as a function of the position in the gap of the Couette cell, for the $0.7 wt\%$ sample with no added salt. (a) Velocity profiles for applied shear rates up to $50 s^{-1}$, and (b) for 50 up to $130 s^{-1}$. The numbers on the right axis indicate the applied shear rate. The dashed curves through the data points are guides-to-the-eye, while the straight lines correspond to the linear profiles near the walls of the shear cell.

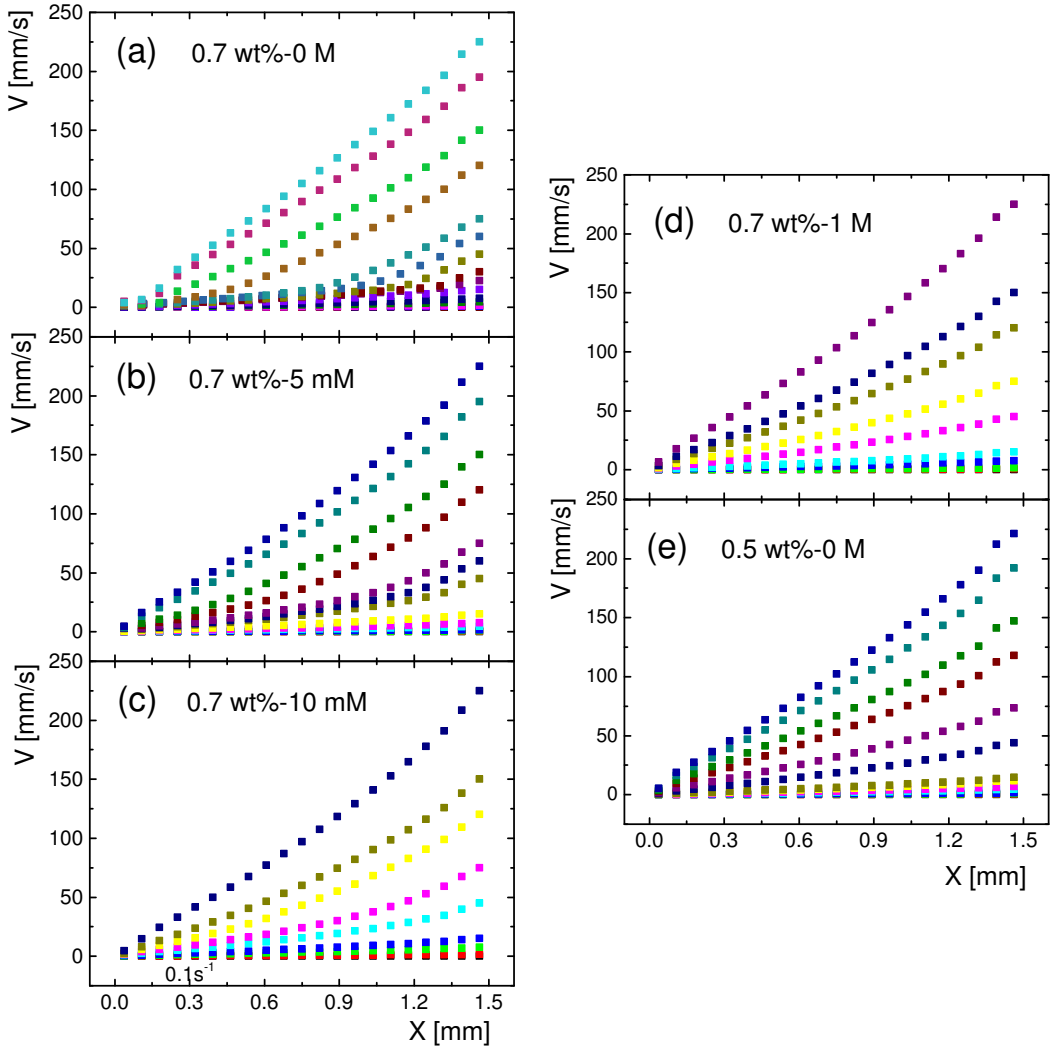

Fig. 4 Velocity profiles at different shear rates, ranging from 0.1 to $150 s^{-1}$, for all investigated samples, at various xanthan concentrations and added salt concentrations, as indicated in the figure.

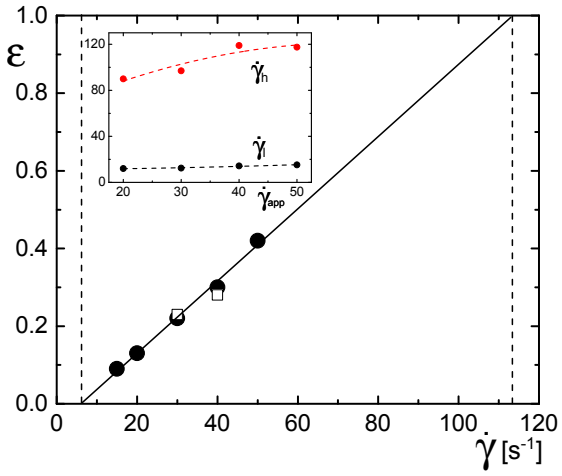

Fig. 5 The lever-rule plot for $0.7\,wt\%$ xanthan without added salt (the solid circles), and for the $5\,mM$ salt (the open squares), where the fraction ε of the volume occupied by the high shear-rate band is plotted against the applied shear rate. The data points are based on the determination of ε from the velocity profiles with a sharp interface. The vertical dashed lines indicate the predicted range $6-113\,s^{-1}$ of applied shear rates where shear-banding occurs. The inset shows the shear rates in the high- and low shear-rate bands as a function of the applied shear rates (in s^{-1}) for the system without added salt.

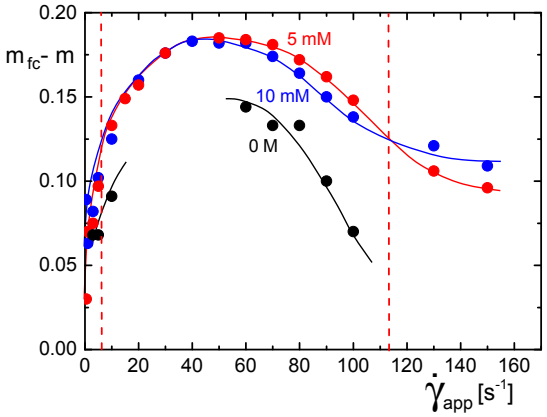

Fig. 6 The difference of the exponents m_{fc} as determined from the flow curve and m as determined from the shear-thinning-function fit for $0.7\,wt\%$ xanthan, with $0M$, $5\,mM$ and $10\,mM$ added salt. The lines are guides-to-the-eye. The gap in the data for the sample without salt is due to the fact that the interface is too sharp to be able to fit the flow curve with the shear-thinning function. Typical errors in the data points are ± 0.05.

absence of slip (like in our samples), the velocity of the rotating inner cylinder is on the one hand equal to $\dot{\gamma}_{app}L$, with $\dot{\gamma}_{app}$ the applied shear rate and L the gap width, and is on the other hand equal to $\dot{\gamma}_l L_l + \dot{\gamma}_h L_h$, with $\dot{\gamma}_h$ and $\dot{\gamma}_l$ the shear rates in the low and high shear-rate band, respectively, and with L_h and L_l the extent of these bands. Since $L = L_h + L_l$, it follows that the fraction of the gap that is occupied with the high shear-rate band is equal to,

$$\varepsilon \equiv \frac{L_h}{L} = \frac{\dot{\gamma}_{app} - \dot{\gamma}_l}{\dot{\gamma}_h - \dot{\gamma}_l}\,. \qquad (1)$$

This lever-rule predicts that the extent of the high shear-rate band varies linearly with the applied shear rate, in case the shear rates within the bands are insensitive to the applied shear rate. The extent of the high shear-rate band vanishes at the lower boundary of the shear-rate region where banding occurs (where $\dot{\gamma}_{app} = \dot{\gamma}_l$), and is equal to the full gap width L at the upper boundary (where $\dot{\gamma}_{app} = \dot{\gamma}_h$). An accurate determination of the shear rates within the two shear-bands is only possible when sharp interfaces occur, that is, when the extent of the two bands is sufficiently large to determine the shear rates $\dot{\gamma}_{h,l}$. The lever rule can therefore only be constructed for the lower applied shear rates for the sample $0.7\,wt\%$ without added salt (see Fig.3a), and for two shear rates for the $5\,mM$ added salt. The fraction ε in eq.(1) is plotted against the applied shear rate for these relatively small shear rates in Fig.5. As can be seen from this figure, we recover the predicted linear dependence of ε on the applied shear rate, despite the slight dependence of $\dot{\gamma}_{l,h}$ on the applied shear rate (see the inset in Fig.5). Moreover, the shear-rate range where banding occurs, on the basis of the lever-rule plot in Fig.5, is found to be $6-113\,s^{-1}$ (indicated by the vertical dashed lines in Fig.5). This corresponds to the shear-rate range where the sloped plateau in the flow curve in Fig.1d is found. Since the lever rule cannot cease to be valid at shear rates only half-way the shear-banding region, we conclude that the highly curved flow profiles in Fig.3b correspond to SBI-states with a broad interface.

Another indication that the curved flow profiles correspond to SBI-states, is to compare the observed flow profile with the expected profile for a Couette geometry when the classic shear-banding instability is absent. For a stable, non-SBI-state, for which the stress scales like $\sigma \sim \dot{\gamma}^m$, the exact stationary velocity flow profile in a Couette cell is given by the shear-thinning function[55],

$$V(x) = \omega_0 R_1 [(R_2 - x)^{1-2/m} - R_2^{1-2/m}]/[R_1^{1-2/m} - R_2^{1-2/m}], \qquad (2)$$

where, as before, x is the distance from the stationary outer cylinder with rotational velocity ω_0, and R_1 and R_2 are the radii of the inner and outer cylinder, respectively. The only fit parameter in the shear-thinning function is the shear-thinning parameter m. For Newtonian fluids, the shear-thinning parameter is unity, in which case the velocity in eq.(2) represents the natural geometry-imposed variation of the velocity within the gap of the Couette cell. More pronounced curved flow profiles as compared to Newtonian fluids occur for systems that exhibit shear-thinning. We have seen in the flow curve in Fig.1d, that within the shear-rate range of about $1-110\,s^{-1}$, the stress scales like $\sigma \sim \dot{\gamma}^{m_{fc}}$ with an exponent $m_{fc} \approx 0.20$. The difference between the value of m obtained from fits of highly curved flow profiles to the shear-thinning function (2) and the value of the flow-curve exponent m_{fc} is thus indicative for the occurrence of a SBI-state (but only for applied shear rates where the scaling $\sigma \sim \dot{\gamma}^{m_{fc}}$ holds). When there is no shear-banding instability, m is equal to m_{fc}. This comparison is of course only possible when all flow profiles can be accurately fitted to the shear-thinning function (2), which turns out to be case, except for the profiles with a sharp interface (for which it is evident that these are SBI-state). The difference between the exponent m_{fc} obtained from the flow curve and the

exponent m obtained from fits of the flow profiles to the shear-thinning function, is plotted in Fig.6. The vertical dashed lines indicate the shear-banding region corresponding to SBI-states complying with the lever rule. As can be seen from this plot, for the three samples with $0.7\,w\%$ xanthan without added salt and with 5 and $10\,mM$ added salt, there are significant differences between the two exponents within the shear-banding region (the experimental error in $m_{fc}-m$ is of the order of 0.05). The difference $m_{fc}-m$ remains large beyond the shear-banding region at large applied shear rates, since for those shear rates the scaling $\sigma \sim \dot{\gamma}^{m_{fc}}$ does not hold, so that m is generally not equal to m_{fc} (the sloped plateau in the flow curve in Fig.1d ends at about $110\,s^{-1}$). For the flow curves for the sample with $1\,M$ added salt, the difference between m_{fc} and m is of the order of the experimental error.

The above analysis strongly suggest that the $0.7\,wt\%$ xanthan solutions without salt and with 5 and $10\,mM$ added salt exhibit the classic shear-banding instability, with very broad interfaces between the shear-bands at larger salt concentration. Whether the samples with $1\,M$ added salt, and with the $0.5\,wt\%$ xanthan concentration exhibit SBI-states cannot be answered, since there is the possibility that the interface for these systems is as large, or even larger, than the cell gap width.

Interface widths can be estimated from the flow profiles as follows. For a broad interface, the flow curve can be fitted by the shear-thinning function in eq.(2). An example of such a fit is given in Fig.7a (the red solid line). The width of the interface is estimated from the difference between the actual flow velocity and the linear profiles (the blue lines in Fig.7a) corresponding to the slopes at the inner- and outer cylinder as obtained from the fitted shear-thinning function, as sketched in Fig.7b. For sharp interfaces, like the profile in Fig.7c, the linear blue profiles can be obtained directly from the flow-profile data, after which the same procedure can be used to determine the interface width, as illustrated in Fig.7d. The thus determined interface widths are given in Fig.8 as a function of the applied shear rate. The smallest interface widths are found for the sample without added salt and small applied shear rates, which however still span about $1/3$ of the shear-cell gap. The other two shear-banding samples, with $5\,mM$ and $10\,mM$ added salt, exhibit broader bands, spanning more than $1/2$ of the entire gap.

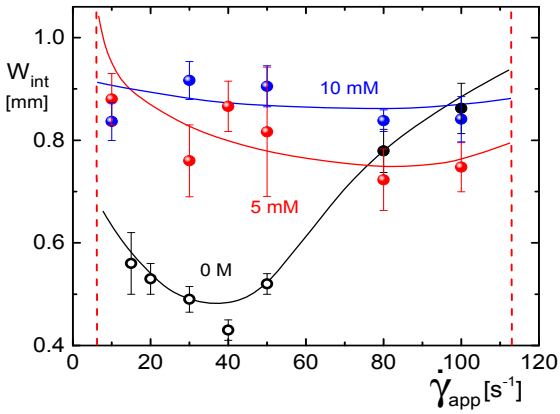

Fig. 8 The width of the shear-band interface as a function of the applied shear rate, for the samples of $0.7\,wt\%$ xanthan without added salt and with 5 and $10\,mM$ added salt. The open points are for sharp interfaces, the filled symbols for broad interfaces. Note that the gap width of the shear cell is $1.5\,mm$. The solid lines are guides-to-the-eye. The vertical dashed lines indicate the shear-banding region as obtained from the lever-rule plot.

5 Diagram-of-States and Birefringence

A diagram-of-states can be constructed, where the various flow profiles that occur are indicated as a function of the added salt concentration and the applied shear rate. Flow profiles could be accurately fitted with the shear-thinning function (2) also for applied shear rates that are outside the shear-rate range where the flow curve exhibits an exponential behaviour (where the stress varies like $\dot{\gamma}^{m_{fc}}$). This can be used to distinguish flow profiles on the basis of the value of the exponent m obtained from such fits. Three flow profiles can be distinguished: (i) profiles for which $m > m_{fc}$, (ii) for which $m < m_{fc}$, and (iii) profiles with sharp interfaces, where m can not be determined because a fit to the shear-thinning function is not possible. The profiles (ii) include banded flows with broad interfaces. The state-diagram in fig.9 shows where these flow profiles are found, depending on the salt concentration and the applied shear rate for the $0.7\,wt\%$ xanthan sample. The vertical red-dashed lines indicate the shear-banding region as obtained from the lever-rule experiments. The solid black lines indicate where the exponent m as obtained from the velocity profile becomes smaller than the shear thinning exponent m_{fc} as obtained from the flow curve. The minimum value of m occurs well within the banding region, and continuously increases away from the banding region. The dashed curve indicates the region where sharp interfaces are observed. For added-salt concentrations larger than a few mM, shear-banding occurs, with broad interfaces.

Birefringence experiments are employed to monitor whether shear-induced structural changes occur. Birefringence was measured between crossed polarizers with increasing shear rate for the $0.7\ wt\%$ xanthan samples. Figure 10 shows the transmitted light intensity through the sample, which is placed between crossed polarizers with polarization directions parallel and perpendicular to the flow direction, as a function of the applied shear rate. Images show the observed birefringence patterns. The transmitted intensity is a measure for the degree of birefringence related to orientation of xanthan chains at angles of 45^o with respect to the flow direction. The observed birefringence increases with shear rate for each ionic strength, as can be seen from Fig.10. The birefringence for the shear-banding samples is significantly larger than for the non-banding system (with $1\,M$ added salt), indicating that significant structural changes occur for the systems that exhibit shear-banding.The larger birefringence intensity is consistent with the crossed birefringent patterns, which are similar to what we observed in supramolecular polymer solution[17]. Exploring the nature of the structural changes requires a separate scattering/microscopy study, which is beyond the scope of the present work.

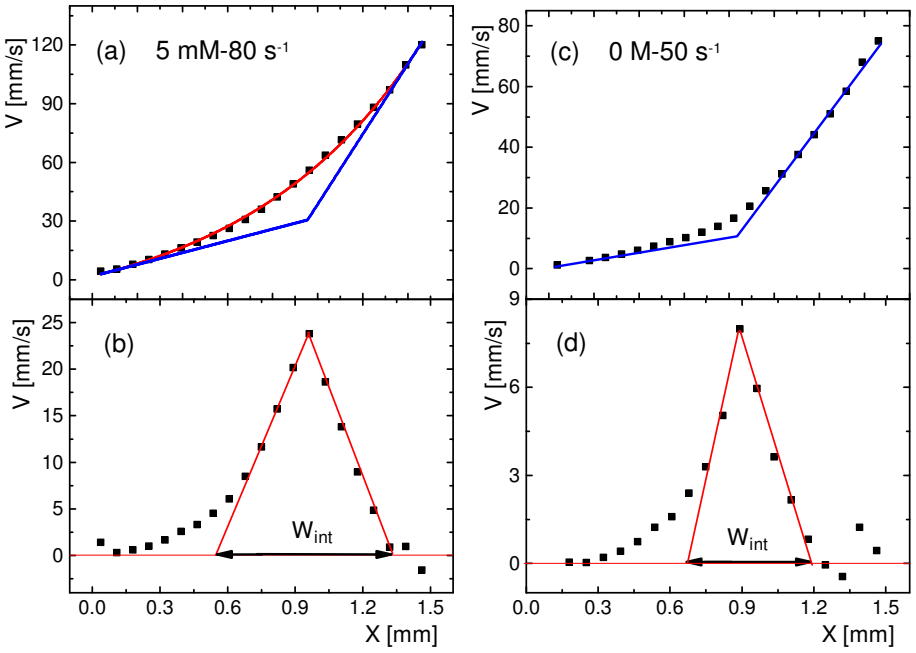

Fig. 7 The determination of interface widths for the $0.7\,wt\%$ Xanthan concentration, for two shear rates. (a) A broad interface with the shear-thinning function fit given by the red curve. The blue lines are linear curves with a slope equal to that of the slope of the shear-thinning function at the walls of the shear cell. Panel (b) illustrates the determination of the width W_{int} of the interface. (c) For a relatively sharp interfaces, the corresponding linear curves in blue are determined directly from the data points near the wall of the cell, so that the same procedure can be used to determine the interface width, as plotted in (d).

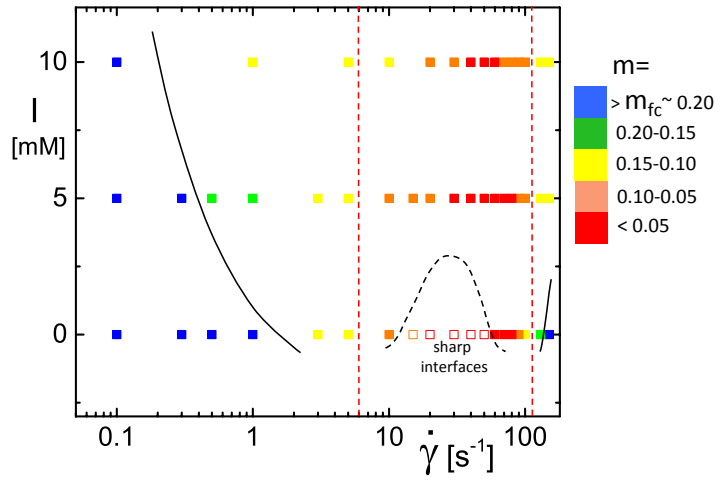

Fig. 9 The diagram-of-states in the added-salt-concentration I versus the shear-rate plane, where flow profiles are distinguished depending on the shear-thinning parameter m. The open points refer to banded profiles with a sharp interface. The vertical dashed lines indicate the shear-banding region as obtained from the lever rule.

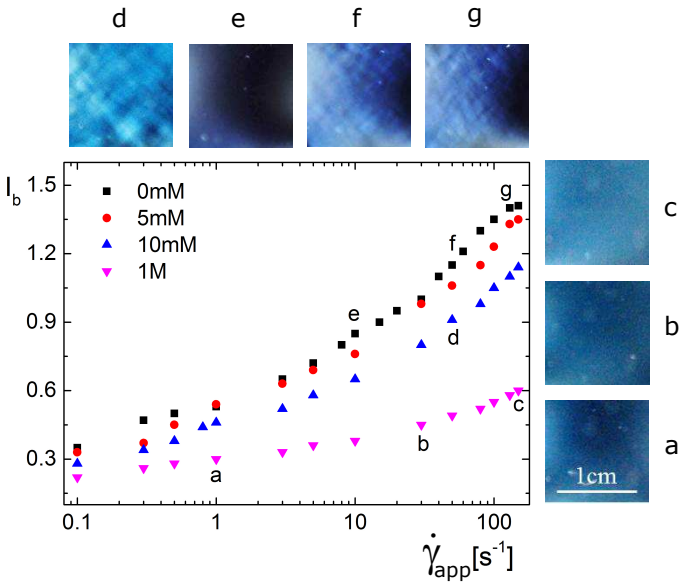

Fig. 10 The transmitted intensity I_s versus the applied shear rate for $0.7\,wt\%$ xanthan solutions at different salt concentrations. The images are taken between crossed polarizers during shear, where the labels indicate to which data points they belong.

6 Discussion and Conclusions

The question addressed in this work is whether highly entangled polymeric systems can exhibit the classic shear-banding instability that complies with strong shear thinning, without necessarily giving rise to a clear shear-banded state but rather to a highly curved flow profile. The common situation in other types of systems, such as surfactant wormlike micelles, is that the flow profiles resulting from the classic shear-banding instability consists of two extended regions (the "bands") within which the shear rate is constant, separated by a sharp interface. We argue on the basis of experiments on xanthan solutions, that polymeric systems can exhibit the classic shear-banding instability, but that the interface can be unusually broad, of the order of the gap width of the shear cell. The occurrence of very broad interfaces possibly justifies the claims in earlier work, where highly curved flow profiles in various types of polymeric systems were interpreted as systems that exhibit the classic shear-banding instability[30,32,46].

We can make this claim because we observe a smooth transition between such stationary flow profiles with sharp bands and curved profiles for concentrated xanthan solutions. The sharply banded flow is found for $0.7\,wt\%$ xanthan solutions at zero added salt in a range of relatively low applied shear rates, while the width of the interface, for which we gave a new definition, increases when moving away from this region in parameter space until the extent of the interface is comparable or larger than the cell gap width and finally becomes linear. This effect has been reported earlier as a function the ionic strength for wormlike micelles[56] and DNA[46], but it had not been quantified in terms of the widening of the interface. The claim that curved profiles can still be considered as shear-banded states, in the sense that they are the result of the classic shear-banding instability, is supported by two main observations. First, the lever-rule plot, as constructed from the profiles with a sharp interface for the lowest ionic strength, is linear as it should. The extrapolation to determine the shear-rate range where banding occurs coincides with the extent of the sloped stress plateau in the flow curve, while the data for 5 mM added salt overlay. Since the lever rule cannot cease to be valid at shear rates only half-way the shear-banding region, we conclude that the highly curved flow profiles in Fig.3b correspond to SBI-states with a broad interface, including the profiles at higher ionic strength. Second, we compared the exponents m and m_{fc}: the former describes the flow profile in a Couette geometry (see eq.2) for a stable fluid for which the stress scales like $\sigma \sim \dot{\gamma}^m$, while the latter characterizes the power-law behaviour of the sloped stress plateau in the flow curve $\sigma \sim \dot{\gamma}^{m_{fc}}$. When the system is stable, the two exponents must be equal. In case the power-law dependence in the flow curve is the result of the shear-banding instability, the two exponents are generally different. We find that the two exponents are indeed different for the 0, 5, $10\,mM$ salt concentrations, indicating that the curved velocity profiles originate from the shear-banding instability. The sample with the very high salt concentration $1\,M$ can not be analyzed in this way, since the difference between the two exponents is within experimental error. A stability diagram is constructed, which summarizes the several flow profiles that occur in the added-salt-concentration versus shear-rate plane.

The fact that samples with very similar flow curves and relaxation dynamics, as witnessed by the scaling behavior of the rheology, produce velocity profiles ranging from sharply banded to curved, suggests that molecular interactions play an important role in shear-band formation and potentially in the widening of the interface. The Rolie-poly model, from which non-linear behavior of polymers can be predicted, provides a local parameter which describes a rate at which entanglements are swept out by flow[7]. This rate could be related either to the increased flexibility or reduced repulsion when increasing the ionic strength. The direct relation between birefringence and shear-band formation, as observed earlier for many other systems, see Fig. 10, suggests that stiffness is a prerequisite for shear-banding. However, similar experiments on DNA suggest that electro-static repulsion facilitates the shear induced alignment[46]. In order to understand the link between molecular interactions and shear-band formation one possibly has to connect the rate at which entanglements are swept out to the ease with which a sharp interface is formed, which is given by the shear curvature viscosity[5] or, equivalently, the stress diffusion coefficient[6]. Better controlled and tunable systems are required to make such a link. Note also that alternatively, widening could also be observed when the interface between the bands becomes unstable[57–60]. Other profiling techniques would need to be applied in order to investigate this possibility.

Finally, we want to evoke awareness with this paper of the possibility of shear-band formation in this relatively ill-defined and heavily studied system. Previously wall slip[61,62] and hints of shear-banding[63] in xanthan solutions have been reported, but this is the first systematic study that identifies a region of shear-banding. This is crucial for the correct interpretation of conventional rheological results, and therefore of industrial importance[42]. These results also extrapolate to many other products that are used as rheology modifiers.

Conflict of interest

There are no conflicts to declare.

Acknowledgements

H.T. acknowledges the China Scholarship Council (NO.201306240056) for financial support. T.K. acknowledges the IHRS BioSoft guest student program for the chance to work on this project. E. Stiakakis and Ch. Lang are thanked for fruitful discussions.

References

1 J. K. G. Dhont and W. J. Briels. Gradient and vorticity banding. *Rheol. Acta*, 47(3):257–281, 2008.

2 P. D. Olmsted. Perspectives on shear banding in complex fluids. *Rheol. Acta*, 47(3):283–300, 2008.

3 T. Divoux, M. A. Fardin, S. Manneville, and S. Lerouge. Shear banding of complex fluids. *Annu. Rev. Fluid. Mech.*, 48(1):81–103, 2016.

4 H. Jin, K. Kang, K. H. Ahn, and J. K. G. Dhont. Flow instability due to coupling of shear-gradients with concentra-

tion: non-uniform flow of (hard-sphere) glasses. *Soft matter*, 10(47):9470 – 9485, 2014.

5 J. K. G. Dhont. A constitutive relation describing the shear-banding transition. *Phys. Rev. E*, 60(4):4534–4544, 1999.

6 P. D. Olmsted, O. Radulescu, and C. Y. D. Lu. JohnsonâĂŞsegalman model with a diffusion term in cylindrical couette flow. *J. Rheol.*, 44(2):257–275, 2000.

7 J. M. Adams, S. M. Fielding, and P. D. Olmsted. Transient shear banding in entangled polymers: A study using the roliepoly model. *J. Rheol.*, 55(5):1007–1032, 2011.

8 S. M. Fielding. Triggers and signatures of shear banding in steady and time-dependent flows. *J. Rheol.*, 60(5):821–834, 2016.

9 S. M. Fielding and P. D. Olmsted. Flow phase diagrams for concentration-coupled shear banding. *Eur. Phys. J. E*, 11(1):65–83, 2003.

10 M. Cromer, M. C. Villet, G. H. Fredrickson, and L. G. Leal. Shear banding in polymer solutions. *PhFl*, 25(5):051703, 2013.

11 J. P. Decruppe, R. Cressely, R. Makhloufi, and E. Cappelaere. Flow birefringence experiments showing a shear-banding structure in a ctab solution. *Colloid. Polym. Sci.*, 273(4):346–351, 1995.

12 J. F. Berret, G. Porte, and J. P. Decruppe. Inhomogeneous shear flows of wormlike micelles:ma master dynamic phase diagram. *Phys. Rev. E*, 55(2):1668–1676, 1997.

13 J. F. Berret, D. C. Roux, and P. Lindner. Structure and rheology of concentrated wormlike micelles [4]at the shear-induced isotropic-to-nematic transition. *The European Physical Journal B - Condensed Matter and Complex Systems*, 5(1):67–77, 1998.

14 M. M. Britton, R. W. Mair, R. K. Lambert, and P. T. Callaghan. Transition to shear banding in pipe and couette flow of wormlike micellar solutions. *J. Rheol.*, 43(4):897–909, 1999.

15 Y. T. Hu and A. Lips. Kinetics and mechanism of shear banding in an entangled micellar solution. *J. Rheol.*, 49(5):1001–1027, 2005.

16 E. Miller and J. Rothstein. Transient evolution of shear-banding wormlike micellar solutions. *Journal of Non-Newtonian Fluid Mechanics*, 143(1):15, 2007.

17 J. van der Gucht, M. Lemmers, W. Knoben, N. A. Besseling, and M. P. Lettinga. Multiple shear-banding transitions in a supramolecular polymer solution. *Phys. Rev. Lett.*, 97(10):108301, 2006.

18 I. Kunita, K. Sato, Y. Tanaka, Y. Takikawa, H. Orihara, and T. Nakagaki. Shear banding in an f-actin solution. *Phy Rev Lett*, 109(24):248303, 2012.

19 B. S. Douglass, R. H. Colby, L. A. Madsen, and P. T. Callaghan. Rheo-nmr of wormlike micelles formed from nonionic pluronic surfactants. *Macromolecules*, 41(3):804–814, 2008.

20 B. Lonetti, J. Kohlbrecher, L. Willner, J. K. G. Dhont, and M. P. Lettinga. Dynamic response of block copolymer wormlike micelles to shear flow. *J. Phys. Condens. Matter*, 20(40):404207–404218, 2008.

21 J. Sprakel, E. Spruijt, M. A. Cohen Stuart, N. A. M. Besseling, M. P. Lettinga, and J. van der Gucht. Shear banding and rheochaos in associative polymer networks. *Soft Matter*, 4(8):1696–1705, 2008.

22 E. V. Menezes and W. W. Graessley. Nonlinear rheological behavior of polymer systems for several shear-flow histories. *J Polym Sci B Polym Phys.*, 20(10):1817–1833, 1982.

23 Y. T. Hu, C. Palla, and A. Lips. Comparison between shear banding and shear thinning in entangled micellar solutions. *J. Rheol.*, 52(2):379–400, 2008.

24 Y. W. Inn, K. F. Wissbrun, and M. M. Denn. Effect of edge fracture on constant torque rheometry of entangled polymer solutions. *Macromolecules*, 38(22):9385–9388, 2005.

25 C. P. Sui and G. B. McKenna. Instability of entangled polymers in cone and plate rheometry. *Rheol. Acta*, 46(6):877–888, 2007.

26 T. Schweizer. Shear banding during nonlinear creep with a solution of monodisperse polystyrene. *Rheol. Acta*, 46(5):629–637, 2007.

27 P. Tapadia and S. Q. Wang. Direct visualization of continuous simple shear in non-newtonian polymeric fluids. *Phys. Rev. Lett.*, 96(1):016001, 2006.

28 P. Tapadia, S. Ravindranath, and S. Q. Wang. Banding in entangled polymer fluids under oscillatory shearing. *Phys. Rev. Lett.*, 96(19):196001, 2006.

29 Y. T. Hu, L. Wilen, A. Philips, and A. Lips. Is the constitutive relation for entangled polymers monotonic? *J. Rheol.*, 51(2):275–295, 2007.

30 P. E. Boukany, S. Q. Wang, S. Ravindranath, and L. J. Lee. Shear banding in entangled polymers in the micron scale gap: a confocal-rheoscopic study. *Soft Matter*, 11(41):8058–8068, 2015.

31 P. E. Boukany, Y. T. Hu, and S. Q. Wang. Observations of wall slip and shear banding in an entangled dna solution. *Macromolecules*, 41(7):2644–2650, 2008.

32 P. E. Boukany and S. Q. Wang. Shear banding or not in entangled dna solutions depending on the level of entanglement. *J. Rheol.*, 53(1):73–83, 2009.

33 P. E. Boukany and S. Q. Wang. Exploring the transition from wall slip to bulk shearing banding in well-entangled dna solutions. *Soft Matter*, 5(4):780–789, 2009.

34 P. E. Boukany and S. Q. Wang. Shear banding or not in entangled dna solutions. *Macromolecules*, 43(17):6950–6952, 2010.

35 K. A. Hayes, M. R. Buckley, I. Cohen, and L. A. Archer. High resolution shear profile measurements in entangled polymers. *Phys. Rev. Lett.*, 101(21):218301, 2008.

36 K. A. Hayes, M. R. Buckley, H. B. Qi, I. Cohen, and L. A. Archer. Constitutive curve and velocity profile in entangled polymers during start-up of steady shear flow. *Macromolecules*, 43(9):4412–4417, 2010.

37 Y. F. Li, M. Hu, G. B. McKenna, C. J. Dimitriou, G. H. McKinley, R. M. Mick, D. C. Venerus, and L. A. Archer. Flow field visualization of entangled polybutadiene solutions under nonlin-

ear viscoelastic flow conditions. *J. Rheol.*, 57(5):1411–1428, 2013.

38 Y. F. Li and G. B. McKenna. Startup shear of a highly entangled polystyrene solution deep into the nonlinear viscoelastic regime. *Rheol. Acta*, 54(9-10):771–777, 2015.

39 W. E. Rochefort and S. Middleman. Rheology of xanthan gum: Salt, temperature, and strain effects in oscillatory and steady shear experiments. *J. Rheol.*, 31(4):337–369, 1987.

40 H. C. Lee and D. A. Brant. Rheology of concentrated isotropic and anisotropic xanthan solutions. 2. a semiflexible wormlike intermediate molecular weight sample. *Macromolecules*, 35(6):2223–2234, 2002.

41 H. C. Lee and D. A. Brant. Rheology of concentrated isotropic and anisotropic xanthan solutions. 1. a rodlike low molecular weight sample. *Macromolecules*, 35(6):2212–2222, 2002.

42 N. B. Wyatt and M. W. Liberatore. Rheology and viscosity scaling of the polyelectrolyte xanthan gum. *J. Appl. Polym. Sci.*, 114(6):4076–4084, 2009.

43 L. Xu, G. Xu, T. Liu, Y. Chen, and H. Gong. The comparison of rheological properties of aqueous welan gum and xanthan gum solutions. *Carbohydr. Polym.*, 92(1):516–522, 2013.

44 L. Zhong, M. Oostrom, M. J. Truex, V. R. Vermeul, and J. E. Szecsody. Rheological behavior of xanthan gum solution related to shear thinning fluid delivery for subsurface remediation. *J. Hazard. Mater.*, 244-245:10, 2013.

45 S. Dumitriu. *Polysaccharides: Structural Diversity and Functional Versatility*. Taylor & Francis, 2 edition, 2004.

46 Y. T. Hu, C. Palla, and A. Lips. Role of electrostatic interactions in shear banding of entangled dna solutions. *Macromolecules*, 41(18):6618–6620, 2008.

47 R. S. Graham, E. P. Henry, and P. D. Olmsted. Comment on âĂIJnew experiments for improved theoretical description of nonlinear rheology of entangled polymersâĂİ. *Macromolecules*, 46(24):9849–9854, 2013.

48 G. Marrucci. Dynamics of entanglements: A nonlinear model consistent with the cox-merz rule. *J Nonnewton Fluid Mech.*, 62(2):279–289, 1996.

49 G. Ianniruberto and G. Marrucci. A simple constitutive equation for entangled polymers with chain stretch. *J. Rheol.*, 45(6):1305–1318, 2001.

50 S. Q. Wang, Y. Y. Wang, S. W. Cheng, X. Li, X. Y. Zhu, and H. Sun. New experiments for improved theoretical description of nonlinear rheology of entangled polymers. *Macromolecules*, 46(8):3147–3159, 2013.

51 T. A. Camesano and K. J. Wilkinson. Single molecule study of xanthan conformation using atomic force microscopy. *Biomacromolecules*, 2(4):1184–1191, 2001.

52 S. A. Rogers, D. Vlassopoulos, and P. T. Callaghan. Aging, yielding, and shear banding in soft colloidal glasses. *Phys. Rev. Lett.*, 100(12):128304, 2008.

53 F. Snijkers, R. Pasquino, P.D. Olmsted, and D. Vlassopoulos. Perspectives on the viscoelasticity and flow behavior of entangled linear and branched polymers. *J. Phys.: Condens. Matter*, 27(47):473002, 2015.

54 J. Delgado, H. Kriegs, and R. Castillo. Flow velocity profiles and shear banding onset in a semidilute wormlike micellar system under couette flow. *J. Phys. Chem. B*, 113(47):15485–15494, 2009.

55 J. B. Salmon, A. Colin, S. Manneville, and F. Molino. Velocity profiles in shear-banding wormlike micelles. *Phys. Rev. Lett.*, 90(22):228303, 2003.

56 D. Gaudino, R. Pasquino, H. Kriegs, N. Szekely, W. Pyckhout-Hintzen, M. P. Lettinga, and N. Grizzuti. Effect of the salt-induced micellar microstructure on the nonlinear shear flow behavior of ionic cetylpyridinium chloride surfactant solutions. *Phys. Rev. E*, 95(3):032603, 2017.

57 S. Lerouge, M. Argentina, and J. P. Decruppe. Interface instability in shear-banding flow. *Phys. Rev. Lett.*, 96(8):088301, 2006.

58 M. A. Fardin, B. Lasne, O. Cardoso, G. GrÃľgoire, M. Argentina, J. P. Decruppe, and S. Lerouge. Taylor-like vortices in shear-banding flow of giant micelles. *Phys. Rev. Lett.*, 103(2):028302, 2009.

59 M. A. Fardin and S. Lerouge. Instabilities in wormlike micelle systems. *Eur. Phys. J. E*, 35(9):91, 2012.

60 M.A. Fardin, L. Casanellas, B. Saint-Michel, S. Manneville, and S. Lerouge. Shear-banding in wormlike micelles: Beware of elastic instabilities. *J. Rheol.*, 60(5):917–926, 2016.

61 S. J. Gibbs, K. L. James, L. D. Hall, D. E. Haycock, W. J. Frith, and S. Ablett. Rheometry and detection of apparent wall slip for poiseuille flow of polymer solutions and particulate dispersions by nuclear magnetic resonance velocimetry. *J. Rheol.*, 40(3):425–440, 1996.

62 M. A. Valdez, L. Yeomans, F. Montes, H. AcuÃśa, and A. Ayala. Influence of temperature on the slip velocity of semidilute xanthan gum solutions. *Rheol. Acta*, 34(5):474–482, 1995.

63 P. T. Callaghan and A. M. Gil. Rheo-nmr of semidilute polyacrylamide in water. *Macromolecules*, 33(11):4116–4124, 2000.